

Fe and Co Complexes of Rigidly Planar Phosphino-Quinoline-Pyridine Ligands for Catalytic Hydrosilylation and Dehydrogenative Silylation

Debashis Basu, Ryan Gilbert-Wilson, Danielle L. Gray,¹ and Thomas B. Rauchfuss^{*1}

School of Chemical Sciences, University of Illinois, Urbana, Illinois 61801, United States

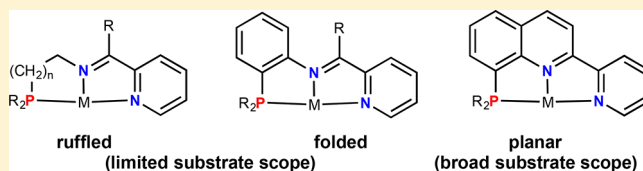
Aswini K. Dash

The Dow Chemical Company, Midland, Michigan 48674, United States

Supporting Information

ABSTRACT: Co and Fe dihalide complexes of a new rigidly planar PNN ligand platform are prepared and examined as precatalysts for hydrosilylation of alkenes. Lithiation of Thummel's 8-bromo-2-(pyrid-2'-yl)quinoline followed by treatment with (*i*-Pr)₂PdCl and (C₆F₅)₂PdCl afforded the phosphine-quinoline-pyridine ligands, abbreviated ^RPQpy for R = *i*-Pr and C₆F₅, respectively. These ligands form 1:1

adducts with the dichlorides and dibromides of iron and cobalt. Crystallographic characterization of FeBr₂(^{iPr}PQpy), FeBr₂(^{ArF}PQpy), CoCl₂(^{iPr}PQpy), CoBr₂(^{iPr}PQpy), and CoCl₂(^{ArF}PQpy) confirmed that the M–P–C–C–N–C–C–N portion of these complexes is planar within 0.078 Å unlike previous generations of PNN complexes where deviations from planarity were ~0.35 Å. Bond distances as well as magnetism indicate that the Fe complexes are high spin and the cobalt complexes are high spin or participate in spin equilibria. Also investigated were the NNN analogues of the ^RPQpy ligands, wherein the phosphine group was replaced by the mesityl ketimine. The complexes FeBr₂(^{Mes}NQpy) and CoCl₂(^{Mes}NQpy) were characterized crystallographically. Reduction of MX₂(^RPQpy) complexes with NaBHET₃ generates catalysts active for anti-Markovnikov silylation of simple and complex 1-alkenes with a variety of hydrosilanes. Catalysts derived from ^{Mes}NQpy exhibited low activity. Fe-^RPQpy derived catalysts favor hydrosilylation, whereas Co-^RPQpy based catalysts favor dehydrogenative silylation. Catalysts derived from CoX₂(^{iPr}PQpy) convert hydrosilanes and ethylene to vinylsilanes. Related experiments were conducted on propylene to give propenylsilanes.



INTRODUCTION

In recent years, hydrosilylation of alkenes using base-metal catalysts has received much attention. Platinum-group metal catalysts are used for all industrial hydrosilylations.¹ In addition to their lower cost, base metal catalysts engage in novel catalytic mechanisms that differ from those observed with traditional platinum group metals. Iron and cobalt catalysts supported by 2,6-diiminopyridine (DIP) ligands effect the hydrosilylation of a broad range of silane and alkene substrates.² Such work implicates a role for sigma-silane complexes as well as redox-noninnocent ligands.³ Striking results have been reported by several groups,^{4–11} as has been summarized.^{12–14} Phosphinite-based catalysts are notable for effecting hydrosilylation of unactivated alkenes in the presence of oxygenic functional groups. Nonbulky DIP-based catalysts exhibit comparable reactivity,¹⁵ signaling that the preference for hydrosilylation vs dehydrosilylation is influenced by steric effects.

Cobalt and iron complexes of phosphine-2-iminopyridine (PNpy) ligands were recently reported by us as catalysts for hydrosilylation.^{16,17} The phosphine-imine-pyridine (PNpy)

platform features the redox noninnocent 2-iminopyridine module as seen in many hydrosilylation catalysts (Figure 1).^{4,21,22} The phosphine substituent provides a strongly anchoring substituent that is tunable electronically and sterically. Upon reduction, FeX₂(PNpy) complexes form catalysts for hydrosilylation of alkenes, but the substrate scope was narrow and the mechanistic insight was limited.¹⁶ Cobalt forms an extensive range of PNpy-based catalysts, and catalytically relevant Co(PNpy)R(L) intermediates could be characterized (R = H, Me, SiPh₂H; L = PPh₃, alkene). The Co-PNpy complexes exhibit excellent activity for the anti-Markovnikov hydrosilylation of 1-octene with Ph₂SiH₂. In the presence of 1-octene and triethoxysilane or heptamethyltrisiloxane, Co(PNpy)-based catalysts preferentially effected alkene isomerization, not hydrosilylation.¹⁷

In this report, we redesigned the PNN platform in an effort to improve performance for hydrosilylation. We also were

Received: June 17, 2018



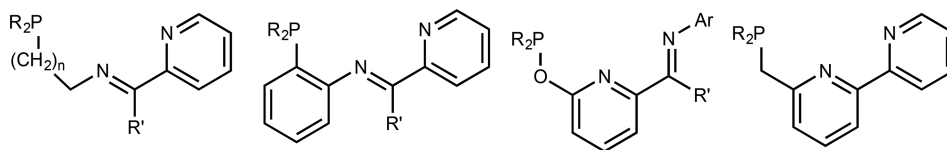
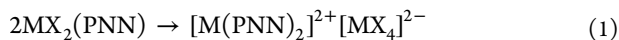


Figure 1. PNN ligand platforms of recent interest in hydrosilylation catalysis.^{4,16–20}

attentive to problems of autoionization, a process that deactivates precatalysts according to eq 1.



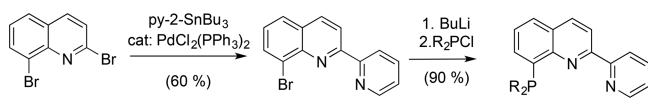
Autoionization can be prevented by the use of bulky substituents,²³ but bulky ligands can be suboptimal for catalysis.¹³ Another way to suppress autoionization is through the use of more rigid ligands that resist ligand exchange.

In searching for an explanation for the modest activity of our previous PNpy-supported complexes, it can be noticed that many active catalysts feature highly planar $\text{M}(\text{CCC})$,⁹ $\text{M}(\text{NNN})$, and $\text{M}(\text{PNN})$ centers.^{13,23} In contrast, previously reported $\text{M}(\text{PNpy})$ complexes have nonplanar MPNN cores owing to the twisted linkage between the phosphine and imine donors. We hypothesized that, with greater planarity, the $\text{M}(\text{PNN})$ center might exhibit enhanced catalytic activity, since planar ligands would stabilize low-spin $\text{Co}(\text{I})$ intermediates.

RESULTS

Part I. Ligands and Coordination Chemistry. Synthesis of PQpy Ligands. A new family of phosphine-quinoline-pyridine ligands, abbreviated PQpy, was prepared. The key intermediate is 8-bromo-2-(pyrid-2'-yl)quinoline, which was prepared from dibromoquinoline (Scheme 1), which in turn

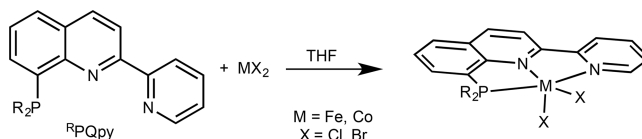
Scheme 1. Synthesis of ^RPQpy Ligands ($\text{R} = i\text{Pr}, \text{C}_6\text{F}_5$)



was obtained by the method of Thummel et al.^{24,25} (Scheme S1, Figures S1–S4). A structurally related NNN ligand platform 8-amino-2-(pyrid-2'-yl)quinoline has been prepared and complexed to Sc.^{26,27} Lithiation of 8-bromo-2-(pyrid-2'-yl)quinoline with butyl lithium gave 8-lithio-2-(pyrid-2'-yl)quinoline, which reacted readily with ^{iPr}Pr₂P-Cl to give the corresponding tertiary phosphine ^{iPr}Pr₂PQpy. Prepared analogously using $(\text{C}_6\text{F}_5)_2\text{P-Cl}$ was the bis(pentafluorophenyl)-phosphine derivative ^{Ar^F}PQpy (Scheme 1). The ^RPQpy ligands are yellow-orange ($\text{R} = i\text{Pr}$) and off-white ($\text{R} = \text{C}_6\text{F}_5$) solids with good solubility in organic solvents. The ¹H NMR spectrum of ^{iPr}Pr₂PQpy in C_6D_6 revealed two methyl multiplets, characteristic of this substituent (Figure S5). Otherwise, the spectrum is well resolved, allowing assignment of the pyridyl vs quinolinyl signals. ³¹P NMR spectra for each phosphine exhibit a singlet (Figure S6). The pentafluorophenyl-containing ligand ^{Ar^F}PQpy was further characterized by ¹⁹F NMR spectroscopy (Figures S7–S9).

^RPQpy Complexes of Fe(II) and Co(II). Combining anhydrous FeBr_2 with THF solutions of ^{iPr}Pr₂PQpy and ^{Ar^F}PQpy in THF afforded the expected ferrous halide complexes (Scheme 2). The neutral $\text{FeBr}_2(\text{iPr}_2\text{PQpy})$ and $\text{FeBr}_2(\text{Ar}^{\text{F}}\text{PQpy})$ complexes are green solids. Solutions of $\text{FeBr}_2(\text{Ar}^{\text{F}}\text{PQpy})$

Scheme 2. Preparation of $\text{MX}_2(\text{R}^{\text{P}}\text{Qpy})$ Precatalysts



deposit reddish solid precipitate, presumably the salt $[\text{Fe}(\text{Ar}^{\text{F}}\text{PQpy})_2]\text{FeBr}_4$, which is poorly soluble in THF. Similar behavior has been observed for $\text{Fe}(\text{II})$ derivatives of a $\text{Ph}_2\text{P-bipy}$ ligand, but complexes derived from ^{iPr}Pr₂P-bpy remain molecular.¹¹

Also prepared were the cobalt(II) complexes $\text{CoCl}_2(\text{iPr}_2\text{PQpy})$, $\text{CoBr}_2(\text{iPr}_2\text{PQpy})$, and $\text{CoCl}_2(\text{Ar}^{\text{F}}\text{PQpy})$. These compounds were obtained as gray-green and blue-green solids. All of these complexes exhibited good solubility in CH_2Cl_2 and MeCN.

The new complexes were characterized spectroscopically and by X-ray crystallography. ¹H NMR spectra for the complexes showed broadened signals between $\delta -30$ and 200 (Figures S10–S13). The paramagnetism of these complexes was assessed by the Evans method on CD_2Cl_2 solutions. The $\text{FeBr}_2(\text{iPr}_2\text{PQpy})$ complex exhibited a magnetic moment of $5.26 \mu_{\text{eff}}$ indicating high-spin Fe^{II} . In the absence of spin–orbit coupling, four unpaired electrons give a moment of $4.90 \mu_{\text{eff}}$. For $\text{CoCl}_2(\text{iPr}_2\text{PQpy})$, the magnetic moment was $4.47 \mu_{\text{eff}}$ consistent with high-spin Co^{II} with three unpaired electrons. In the absence of spin–orbit coupling, three unpaired electrons give a moment of $3.87 \mu_{\text{eff}}$. The complex $\text{CoBr}_2(\text{iPr}_2\text{PQpy})$ does not fit this pattern. Its magnetic moment was only $3.14 \mu_{\text{eff}}$ consistent with an equilibrium mixture of two spin states. Equilibria between high and low spin $\text{Co}(\text{II})$ complexes were long ago observed for other CoX_2L_3 complexes.^{28,29}

These complexes were further characterized by X-ray crystallography (Figure 2, Table 1, Table S1). All metal centers feature a $[\text{N}_2\text{PX}_2]$ coordination environment. The five-coordinate geometries were analyzed using the geometry index τ_5 ,³⁰ which was found to be 0.4260 and 0.1036, for $\text{FeBr}_2(\text{iPr}_2\text{PQpy})$ and $\text{FeBr}_2(\text{Ar}^{\text{F}}\text{PQpy})$, respectively (Table 2). In ideal square pyramidal and trigonal bipyramidal geometries, the τ_5 values are 0 and 1, respectively. Thus, the geometry of the ^{iPr}Pr₂P-containing complex is intermediate between square pyramidal and trigonal bipyramidal, whereas the geometry of the ^{Ar^F}P-containing derivative approaches ideal square pyramidal.³⁰ Crystallography confirms that the Fe-N-N-P atoms are coplanar within 0.078 \AA (Table 2). For the previously published $\text{FeCl}_2(\text{Ph}^{\text{C}}\text{C}^{\text{H}}\text{Ph}^{\text{N}}\text{py})$, the deviation was 0.373 \AA .¹ All of the Fe-N (both quinoline and pyridine N) bond lengths were found to be between 2.14 and 2.19 \AA , whereas the Fe-P bond distances for both complexes were 2.50–2.52 \AA .

Greenish $\text{CoCl}_2(\text{iPr}_2\text{PQpy})$, $\text{CoCl}_2(\text{Ar}^{\text{F}}\text{PQpy})$, and $\text{CoBr}_2(\text{iPr}_2\text{PQpy})$ were also characterized crystallographically (Figure 3, Table 1). The $\text{Co}(\text{II})$ centers are also

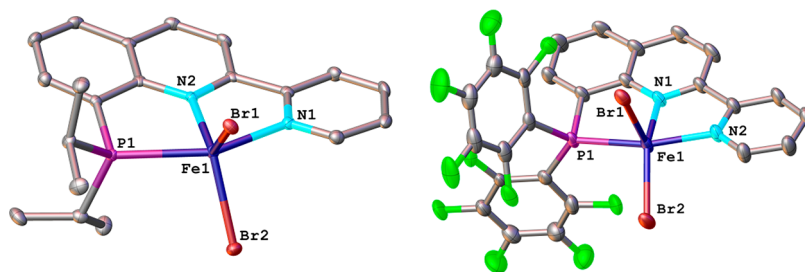


Figure 2. ORTEP representations of $\text{FeBr}_2(\text{iPrPQpy})$ (left) and $\text{FeBr}_2(\text{ArF-PQpy})$ (right), with thermal ellipsoids set at the 50% probability level. H atoms omitted for clarity.

Table 1. Metal–Ligand Bond Lengths (Å) for New Complexes

	$\text{FeBr}_2(\text{iPrPQpy})$	$\text{FeBr}_2(\text{ArF-PQpy})$	$\text{CoCl}_2(\text{iPrPQpy})$	$\text{CoBr}_2(\text{iPrPQpy})$	$\text{CoCl}_2(\text{ArF-PQpy})$
M–N(Q)	2.1879(18)	2.185(2)	2.0971(12)	1.909(4)	2.086(3)
M–N(Py)	2.1527(18)	2.144(2)	2.1380(12)	1.981(4)	2.100(3)
M–P1	2.5020(6)	2.5205(7)	2.4424(4)	2.1985(12)	2.5056(11)
M–hal1	2.4898(4)	2.4719(5)	2.3176(4)	2.5548(7)	2.3035(9)
M–hal2	2.4696(4)	2.4217(4)	2.3001(4)	2.3636(7)	2.3422(9)

Table 2. Planarity Parameters and Tau Values for Fe(II) and Co(II) Complexes

complex	planarity parameter ^a	τ value
$\text{FeBr}_2(\text{iPrPQpy})$	0.078	0.4260
$\text{FeBr}_2(\text{ArF-PQpy})$	0.076	0.1036
$\text{CoCl}_2(\text{iPrPQpy})$	0.038	0.4396
$\text{CoBr}_2(\text{iPrPQpy})$	0.054	0.1613
$\text{CoCl}_2(\text{ArF-PQpy})$	0.040	0.2676
$\text{FeCl}_2(\text{Ph}^{\text{C6H4}}\text{N}^{\text{Ph}}\text{py})^b$	0.373	0.3575
$\text{CoCl}_2(\text{Ph}^{\text{C3}}\text{N}^{\text{Ph}}\text{py})^c$	0.487	0.6781
$\text{CoCl}_2(\text{Ph}^{\text{C6H4}}\text{N}^{\text{Ph}}\text{py})^c$	0.366	0.4748

^aRMSD (Å) for the plane created by M–P–C–C–N(Q)–C–C–N(py) atoms. ^bPrevious work. ^cPrevious work.²

pentacoordinate, with $[\text{N}_2\text{P}(\text{halide})_2]$ coordination environments. The τ_5 values determined for these complexes were 0.4396, 0.1613, and 0.2676 for $\text{CoCl}_2(\text{iPrPQpy})$, $\text{CoBr}_2(\text{iPrPQpy})$, and $\text{CoCl}_2(\text{ArF-PQpy})$, respectively (Table 2). Thus, the $\text{CoCl}_2(\text{iPrPQpy})$ complexes adopt an intermediate geometry between square pyramidal and trigonal bipyramidal, whereas $\text{CoBr}_2(\text{iPrPQpy})$ and $\text{CoCl}_2(\text{ArF-PQpy})$ approach a more ideal square-pyramidal geometry. The planarity deviation (RMSD/Å) imposed by the quinoline, pyridine, and phosphorus atom bound to the metal centers was found to be 0.038, 0.054, and 0.040, for $\text{CoCl}_2(\text{iPrPQpy})$, $\text{CoBr}_2(\text{iPrPQpy})$, and $\text{CoCl}_2(\text{ArF-PQpy})$, respectively (Table 2), which makes these complexes considerably more planar than the previously published $\text{CoCl}_2(\text{Ph}^{\text{C3}}\text{N}^{\text{Ph}}\text{py})$ and $\text{CoCl}_2(\text{Ph}^{\text{C6H4}}\text{N}^{\text{Ph}}\text{py})$ complex (RMSD/Å = 0.487 and 0.366, respectively) (Table 2).² The cobalt(II) chloride and bromide complexes have shown considerable differences in bond lengths. The Co–N(py), Co–N(Q), and Co–P bond lengths are significantly shorter (~ 0.2 Å) in $\text{CoBr}_2(\text{iPrPQpy})$ than in $\text{CoCl}_2(\text{iPrPQpy})/\text{CoCl}_2(\text{ArF-PQpy})$ (Table 1). The crossover from high to low spin in pentacoordinate cobalt(II) complexes is known to be sensitive, e.g., to the identity of the halide.^{28,29} Since these dihalides are precatalysts, their ground states have little bearing on the catalysis observed for their Co(I) derivatives except that the observation of low spin configuration suggests that the PQpy ligands exert a stronger ligand field than the PNpy ligand reported previously.^{16,2}

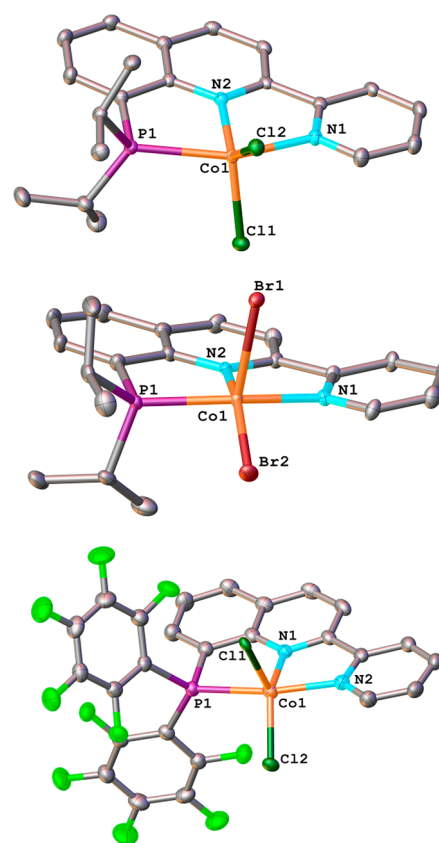
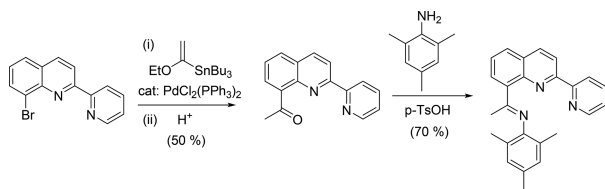


Figure 3. ORTEP representations of $\text{CoCl}_2(\text{iPrPQpy})$ (top), $\text{CoBr}_2(\text{iPrPQpy})$ (middle), and $\text{CoCl}_2(\text{ArF-PQpy})$ (bottom), with thermal ellipsoids set at the 50% probability level. H atoms omitted for clarity.

MesNQpy Ligand and Fe(II) and Co(II) Complexes. Also investigated were the NNN analogues of the ^RPQpy ligands, wherein the phosphine group was replaced by the mesityl ketimine. The required ketone was generated by Stille coupling between 8-bromo-2-(pyrid-2'-yl)quinoline and tributyl(1-ethoxyvinyl)stannane. Hydrolysis gave 8-acetyl-2-(pyrid-2'-yl)quinoline following a literature procedure.²³ Condensation

of this ketone with 2,4,6-trimethylaniline afforded the corresponding imine, labeled $^{\text{Mes}}\text{NQpy}$ (Scheme 3). The ligand was characterized by ^1H NMR spectroscopy (Figure S14).

Scheme 3. Synthesis of the $^{\text{Mes}}\text{NQpy}$ Ligand

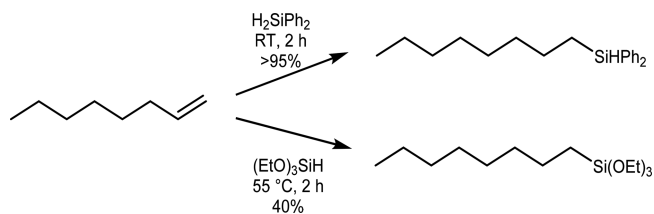


The ligand $^{\text{Mes}}\text{NQpy}$ formed 1:1 adducts with FeBr_2 and CoCl_2 , comparable to the PQpy complexes described above. The Fe complex is green, whereas the cobalt complex is yellow. They are paramagnetic (Figures S15 and S16) and high-spin. The structures of $\text{FeBr}_2(^{\text{Mes}}\text{NQpy})$ and $\text{CoCl}_2(^{\text{Mes}}\text{NQpy})$ were characterized by X-ray crystallography (Figure 4, Tables S2 and S3), which established that they are pentacoordinated. Both complexes are pseudo trigonal bipyramidal (τ for $\text{FeBr}_2(^{\text{Mes}}\text{NQpy})$, 0.5516; τ for $\text{CoCl}_2(^{\text{Mes}}\text{NQpy})$, 0.6978); whereas both of them seem to be less planar (RMSD/Å for the plane created by M–N(im)–C–C–N(Q)–C–C–N(Py) atoms for $\text{FeBr}_2(^{\text{Mes}}\text{NQpy})$, 0.296; for $\text{CoCl}_2(^{\text{Mes}}\text{NQpy})$, 0.290) than their corresponding PQpy analogues.

Part II. Silylation Catalysis. 1-Octene. The new Fe-PQpy complexes were examined initially as catalysts for the hydrosilylation of 1-octene. This substrate allows assessment of the three likely reaction pathways, hydrosilylation (Markovnikov vs the more desirable anti-Markovnikov), dehydrogenative silylation, and alkene isomerization. Following literature precedent,^{14,17,23} the FeBr_2 and CoCl_2 complexes were reductively activated by treatment with 2 equiv of NaBHET_3 in the presence of both alkene and silane substrates. The $\text{Fe-}^{\text{iPr}}\text{PQpy}$ catalyst was effective for the anti-Markovnikov addition of Ph_2SiH_2 at room temperature (Scheme 4). With triethoxysilane, the rate was lower even at elevated temperatures, and competing isomerization to 2-octene was observed. The $\text{Fe-}^{\text{iPr}}\text{PQpy}$ complex also showed promising activity toward heptamethyltrisiloxane ($\text{Me}(\text{Me}_3\text{SiO})_2\text{SiH}$, HMTS) (55 °C, 30% conversion in 2 h, Table 3).

In contrast to the behavior of the Fe-based catalysts, the $\text{Co-}^{\text{iPr}}\text{PQpy}$ catalyst gave unsaturated as well as saturated silanes. On the basis of NMR analysis, the reaction of 1-octene

Scheme 4. Hydrosilylation of 1-Octene with 1 mol % $\text{FeBr}_2(^{\text{iPr}}\text{PQpy})$ -Based Catalyst



and Ph_2SiH_2 gave mainly the allylsilane (71%). Fe- and Co-NQpy-based complexes are inferior catalysts.

Vinylsiloxanes. As a more industrially relevant pair of substrates, HMTS and $\text{Me}_3\text{SiOSiMe}_2\text{CH}=\text{CH}_2$ (VPMDS) were next examined (Scheme 5, Table 4, Figure S17). The $\text{Fe-}^{\text{iPr}}\text{PQpy}$ -based catalyst remains highly active, but hydrosilylation was accompanied by significant dehydrogenative silylation. Yields for dehydrogenative silylation and hydrogenation are similar, as is typical for dehydrogenative silylation. We verified that the Fe catalyst did not catalyze the hydrogenation of 1-octene with 2 atm of H_2 under the conditions of the hydrosilylation experiment.

$\text{Co-}^{\text{iPr}}\text{PQpy}$ -based catalysts were also active but exclusively gave the dehydrogenative products. Catalysis in an open flask (inside a glovebox) gave similar results, indicating that molecular hydrogen, if it is formed, is uninvolved in the reaction. Dehydrogenative silylation is often exhibited by cobalt-DIP catalysts.^{15,31} It is interesting that both $^{\text{iPr}}\text{P-}$ and $(\text{C}_6\text{F}_5)_2\text{P-}$ -based cobalt catalysts function similarly, even though they differ greatly in the hydrosilylation of ethylene (see below). Reduction of $\text{CoCl}_2(^{\text{Mes}}\text{NQpy})$ gave poor catalysts (15% conversion in 2 h, 65 °C).

Ethylene. The finding that the $\text{Co-}^{\text{iPr}}\text{PQpy}$ catalysts were active for dehydrogenative silylation (Table 4) led to an investigation of their use for producing vinylsilanes from silanes and ethylene. Vinylsilanes are versatile reagents, as they can be polymerized, undergo alkene metathesis, are amenable to hydrosilylation, and serve as vinyl transfer agents.^{32–35} Vinylsilanes are prepared by hydrosilylation of acetylene as well as reaction of vinyl lithium with silyl halides.^{36,37} Dehydrogenative silylation has rarely been applied to their preparation.³⁶ It is known that ethylene and $\text{HSi}(\text{OEt})_3$ react to give $\text{EtSi}(\text{OEt})_3$,^{38,39} but the conversion to $\text{CH}_2=\text{CHSi}(\text{OEt})_3$ would be of greater interest.⁴⁰

Reactions were conducted under 2 atm of ethylene at 70 °C using triphenylsilane, HMTS, and triethoxysilane (Figure S18, Table 5). Conversions are almost complete in 2 h at 70 °C.

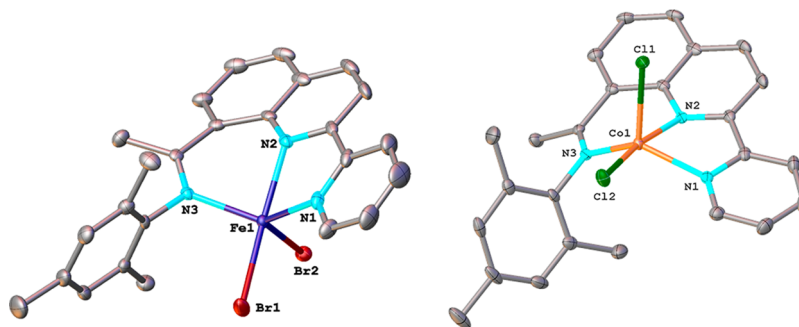


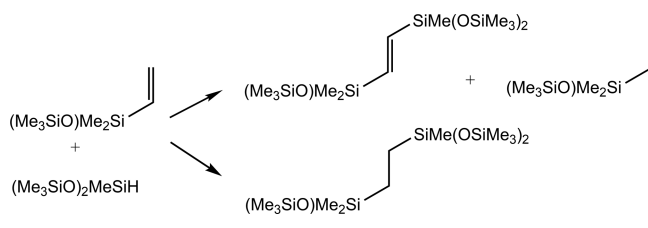
Figure 4. ORTEP representations of $\text{FeBr}_2(^{\text{Mes}}\text{NQpy})$ (left) and $\text{CoCl}_2(^{\text{Mes}}\text{NQpy})$ (right), with thermal ellipsoids set at the 50% probability level. H atoms omitted for clarity.

Table 3. Results of Hydrosilylation of 1-Octene with Fe- and Co-Based Catalysts and Hydrosilanes^a

precatalyst (conditions)	hydrosilane	convn %	C ₈ H ₁₇ SiR ₃ (hydrosilylation)	dehydrogenative silylation	2-octene
Fe- ⁱ PrPQpy (25 °C, 1%, 2 h)	H ₂ SiPh ₂	95	95	0	0
Fe- ⁱ PrPQpy (55 °C, 1%, 2 h)	HMTS	30	30	0	0
Fe- ⁱ PrPQpy (55 °C, 1%, 2 h)	HSi(OEt) ₃	100	40	0	60
Co- ⁱ PrPQpy (25 °C, 1%, 2 h)	H ₂ SiPh ₂	100	19	71 (10) ^b	0
Fe-NQpy (25 °C, 1%, 2 h)	H ₂ SiPh ₂	10	0	0	10

^aYields determined by NMR spectra vs internal integration standard. ^b71% allyl silanes, 10% vinyl silanes, with corresponding amount of octane.

Scheme 5. Products from Catalyzed Reaction of HMTS and VPMDS



The selectivity for vinylsilanes is good (60–85%) for the ⁱPr₂P-based Co catalysts. Whereas the Co-catalyzed reaction of VPMDS + HMTS resulted in no hydrosilylation (only dehydrogenative products), some hydrosilylation is observed with ethylene (Scheme 6). We conclude that the unhindered Co-CH₂CH₂SiR₃ intermediate is more susceptible to attack by hydrosilane (R₃SiH) than is Co-CH(SiR'₃)CH₂R. We confirmed that Fe(PQpy)-based catalysts strongly favored hydrosilylation using the same substrates (Table 5). The ratio of dehydro vs hydrosilylation was reversed when changing from ⁱPr₂P- to (C₆F₅)₂P-based catalyst. This change may indicate the tendency of a less bulky catalyst to favor hydrosilylation vs dehydrogenative silylation.¹⁴

Using the Co-^{Mes}NQpy catalyst under similar conditions, the C₂H₄ + Ph₃SiH reaction also gave largely the ethylsilane. As a benchmark, the Co(DIP^{Mes})Cl₂-derived catalyst was evaluated (DIP^{Mes} = bis mesitylimine of 2,6-diiminopyridine). This catalyst is highly active for a wide range of substrates, although experiments with ethylene were not reported.³¹ When activated with NaBHET₃, this catalyst generates mainly hydrosilylation product with ethylene and triethoxysilane.

Ethylene was investigated as a possible sacrificial substrate³⁶ in dehydrogenative silylations. The idea was tested by conducting the reaction VPMDS + HMTS in the presence and absence of 2 atm of C₂H₄. The ratio of dehydrosilylated/hydrosilylated products was however relatively unaffected.

Table 4. Results of Hydrosilylation of VPMDS with HMTS^a

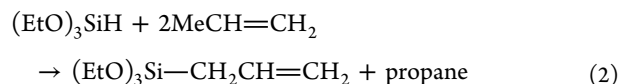
catalyst	T (°C)	convn %	-CH ₂ CH ₂ - (hydrosilylation)	-CH=CH- (dehydrogenative silylation)	-CH ₂ -CH ₃ (hydrogenation)
Fe- ⁱ PrPQpy (1%)	25	95	42	34	24
Fe- ⁱ PrPQpy (1%)	65	>99	21	39	39
Fe- ⁱ PrPQpy (0.5%)	-30 to 25	39	65	17	17
Co- ⁱ PrPQpy (0.5%)	25	60	0	44	56
Co- ⁱ PrPQpy (0.5%)	65	99	0	43	57
Co- ^{ArF} PQpy (0.5%)	65	99	0	46	54
Co- ⁱ PrPQpy (0.5%) + 2 atm of C ₂ H ₄	65	99	0	40	60

^aConditions: MX₂(^RPQpy), NaBHET₃ (2 times catalyst), 1 mmol of alkene, 1 mmol of silane, 2 h. Yields determined by NMR spectroscopy vs internal integration standard.

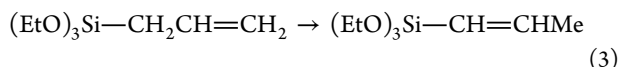
Propylene. The reaction of hydrosilanes with propylene was examined as a potential route of allylsilanes. Allylsilanes are of significant value in organic synthesis.^{41–43} Six products are possible from the reaction of a hydrosilane and propylene, four involving dehydrogenative pathways (Scheme 7).

The dehydrogenative silylation of propene to give triethoxyallylsilane has been achieved with DIP-Co catalysts (98% yield, 23 °C, 0.5 mol % catalyst).⁴⁴ With the Co-ⁱPrPQpy catalyst, 90% conversion required 2 h (2 mol %, 70 °C), but the product was largely *trans*-propenylsilane. Control experiments showed that Co-ⁱPrPQpy catalysts rapidly isomerize allyltriethoxysilane to the propenyl derivative at 70 °C (eq 2–3).

Dehydrogenative silylation:



Isomerization:



Only when the Co(ⁱPrPQpy)-catalyzed reaction was conducted under mild conditions (room temp, 2 h) were traces of the allylsilane detected. Thus, Co-catalyzed isomerization of the intermediate allylsilane is faster than the Co-catalyzed dehydrogenative silylation. In this situation, however, HSi(OEt)₃ is a reluctant substrate, as reflected by the higher temperature (70 °C) required for catalysis. With a more reactive substrate, Ph₃SiH, dehydrogenative silylation proceeds to exclusively give the allylsilane (eq 4).

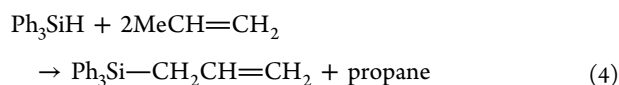
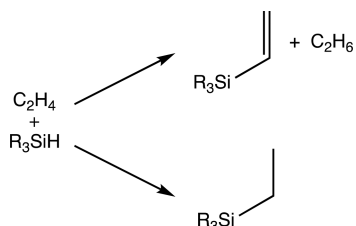


Table 5. Results for Reaction of Ethylene with Various Silanes^a

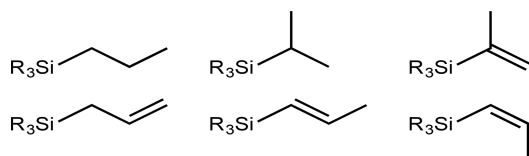
hydrosilane	catalyst	convn %	—CH ₂ CH ₂ — (hydrosilylation)	—CH=CH— (dehydrogenative silylation)
Ph ₃ SiH	Fe- ^{iPr} PQpy	95	75	25
(EtO) ₃ SiH	Fe- ^{iPr} PQpy	85	90	10
HMTS	Fe- ^{iPr} PQpy	85	95	5
Ph ₃ SiH	Co- ^{ArF} PQpy	95	95	5
Ph ₃ SiH	Co- ^{iPr} PQpy	95	15	85
(EtO) ₃ SiH	Co- ^{iPr} PQpy	90	40	60
HMTS	Co- ^{iPr} PQpy	85	14	86
Ph ₃ SiH	Co- ^{Mes} NQpy	90	95	5
(EtO) ₃ SiH	Co-DIP ^{Mes}	99	95	5

^aConditions: MX₂(^RPQpy) (2 mol %), NaBHET₃ (2.2 equiv), 0.5 mmol of silane, 2 h, 2 mL of toluene, saturated with 2 atm of C₂H₄. Experiments were conducted at constant pressure. Results shown are the average of two or three experiments.

Scheme 6. Products from Catalyzed Reaction of Hydrosilanes and Ethylene



Scheme 7. Possible Products from Hydro/Dehydrogenative Silylation of Propylene



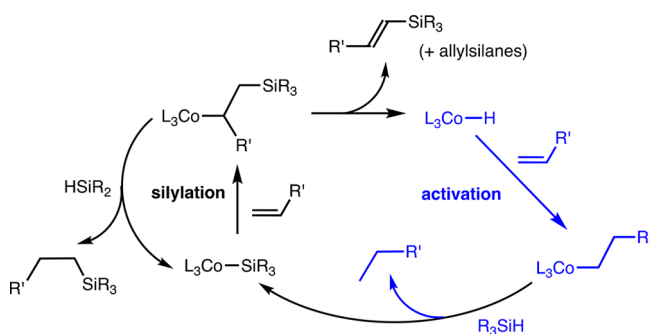
CONCLUSIONS

This paper introduces a new P–N–N ligand platform. The design exploits synthetic routes to the 8-functionalized 2-pyridylquinolines.¹¹ Labeled ^RPQpy, the resulting tridentate PNN ligands embrace the metal by two five-membered chelate rings. As established by several crystallographic studies, the resulting complexes feature highly planar MPNN cores. Illustrating the versatility of 8-bromo-2-pyridylquinoline, a related NNN ligand was prepared by Schiff base condensation of 8-acetyl-2-pyridylquinoline. The resulting imine forms complexes with ruffled meridional MNNN cores with five- and six-membered chelate rings.

All of the complexes are precatalysts for hydrosilylation of alkenes. The activity of the ^RPQpy complexes was higher, and these complexes, especially those based on cobalt, were the focus of catalytic studies. Together with our previous report on more flexible PNN ligands,^{16,17} the present results show that catalytic activity is highly sensitive to the ligand backbone. The quinoline-based PQpy ligands vs PNN ligands based on aldimines both coordinate in a meridional manner, but the M(PQpy) cores are almost perfectly planar. We hypothesize that strictly planar tridentate ligands stabilize low-spin complexes of Co(I), which more effectively bind alkenes than does high-spin Co(I). Although the activities (50–70 °C, 0.5–2% loading) of the new Co complexes are good, they are less active than catalysts based on cobalt-diiminopyridines¹² and nickel-diimines.^{10,14}

Most results can be rationalized by the mechanism shown in Scheme 8.¹⁴ The mechanism invokes the modified Chalk–

Scheme 8. Proposed Mechanism for Reaction of Alkenes with Hydrosilanes in the Presence of Co-PQpy Catalysts



Harrod pathway wherein alkene inserts into the M–Si bond.⁴⁵ With two alkene insertion steps, the mechanism is amenable to the use of sacrificial alkenes, which absorb the equivalent of H₂, although attempted use of ethylene as such a sacrificial agent was unsuccessful.

Seeking novel applications of the new catalysts, we sought to exploit the dehydrogenative silylation with a focus on converting ethylene into vinyl silanes.^{46,47} Prior syntheses of vinylsilanes from ethylene employed precious metal catalysts.^{38,39,48–50} The use of nonprecious metal catalysts for the preparation of vinylsilanes appears to be a fertile direction, and one where first row metals may offer advantages over platinum group catalysts.^{40,51}

EXPERIMENTAL SECTION

General. Liquid silanes, siloxanes, and alkenes were deoxygenated and stored in a nitrogen-filled glovebox, where reactions were also conducted. Research purity ethylene was obtained from Airgas. Solvents (HPLC grade) were treated with a MBraun solvent purification system and stored over 4 Å molecular sieves. ¹H, ³¹P, and ¹⁹F NMR spectra were recorded with a Bruker B-500 spectrometer at 25 °C. Chemical shifts are reported in ppm and coupling constants in Hz. CHN analyses were performed by the School of Chemical Sciences Microanalysis Laboratory using Exeter Analytical CE 440 and PerkinElmer 2440, Series II instruments.

^{iPr}PQpy. A solution of 8-bromo-2-(pyrid-2'-yl)quinoline¹¹ (1.50 g, 5.26 mmol) in THF (100 mL) was cooled to –95 °C. To the cold solution was added a solution of BuLi in hexane (1.6 M, 3.6 mL, 5.76 mmol) dropwise over a period of 15 min, resulting in a color change to pale red, darkening upon completion of the addition. The flask was allowed to warm to –78 °C and was maintained at that temperature for 20 min. The solution of the lithiated heterocycle was added via

cannula over a period of 10 min to a solution of ${}^i\text{Pr}_2\text{P}(\text{Cl})$ (806 mg, 5.28 mmol) in THF (100 mL) at $-95\text{ }^\circ\text{C}$. The reaction solution appeared dark green. After stirring at $-95\text{ }^\circ\text{C}$ for 20 min, the solution was allowed to slowly warm to room temperature, resulting in a color change to red. This solution was maintained for 48 h at room temperature, before volatiles were removed under reduced pressure. The dark red residue was extracted into toluene (100 mL), which was filtered through a plug of basic alumina to give a yellow solution. Removal of volatiles under reduced pressure gave ${}^i\text{PrPQpy}$ as a thick orange oil, which solidified on standing (1.67 g, 5.18 mmol, 98% yield). ${}^{31}\text{P}$ NMR (202 MHz, C_6D_6): δ 3.4 (1P, s br); ${}^1\text{H}$ NMR (500 MHz, C_6D_6): δ 9.15 (1H, ddd, ${}^3J_{\text{H-H}} = 7.9$, ${}^4J_{\text{H-H}} = 1.2$, ${}^5J_{\text{H-H}} = 0.9$, H_a); 8.92 (1H, d, ${}^3J_{\text{H-H}} = 8.6$, H_b); 8.57 (1H, ddd, ${}^3J_{\text{H-H}} = 4.7$, ${}^4J_{\text{H-H}} = 1.8$, ${}^5J_{\text{H-H}} = 0.9$, H_d); 7.75 (1H, ddd, ${}^3J_{\text{H-H}} = 7.0$, ${}^3J_{\text{H-P}} = 4.6$, ${}^4J_{\text{H-H}} = 1.3$, H_i); 7.70 (1H, d, ${}^3J_{\text{H-H}} = 8.6$, H_c); 7.38 (1H, dd, ${}^3J_{\text{H-H}} = 8.0$, ${}^4J_{\text{H-H}} = 1.3$, H_g); 7.31 (1H, ddd, ${}^3J_{\text{H-H}} = 7.9$, ${}^3J_{\text{H-H}} = 7.5$, ${}^4J_{\text{H-H}} = 1.8$, H_k); 7.20 (1H, dd, ${}^3J_{\text{H-H}} = 8.0$, ${}^3J_{\text{H-H}} = 7.0$, H_h); 6.71 (1H, ddd, ${}^3J_{\text{H-H}} = 7.5$, ${}^3J_{\text{H-H}} = 4.7$, ${}^4J_{\text{H-H}} = 1.2$, H_c); 2.54 (2H, qdd, ${}^3J_{\text{H-H}} = 7.0$, ${}^3J_{\text{H-H}} = 7.0$, ${}^3J_{\text{H-P}} = 1.6$, H_j); 1.26 (6H, dd, ${}^3J_{\text{H-P}} = 13.8$, ${}^3J_{\text{H-H}} = 7.0$, H_l); 1.04 (6H, dd, ${}^3J_{\text{H-P}} = 12.0$, ${}^3J_{\text{H-H}} = 7.0$, H_i).

${}^{\text{ArF}}\text{PQpy}$. A solution of 8-bromo-2-(pyrid-2'-yl)quinoline (500 mg, 1.75 mmol) in THF (10 mL) was frozen in a glovebox cold well before a solution of BuLi in hexane (1.6 M, 1.15 mL, 1.84 mmol) was added dropwise over a period of 5 min to the thawing solution, resulting in a color change to red. The solution was stirred for 3 min before being refrozen in the cold well. The solution was removed from the cold well, and as it thawed, it was added dropwise over a period of 5 min to a stirred solution of $(\text{C}_6\text{F}_5)_2\text{PBr}$ (783 mg, 1.76 mmol) in thawing THF (10 mL), which had been frozen in the cold well. Once addition was complete, the resulting solution was allowed to slowly warm to room temperature. This solution was stirred for 16 h at room temperature, before all volatiles were removed under reduced pressure to give a pale residue. The residue was extracted into CH_2Cl_2 (2×30 mL), and the extract was evaporated. After washing the pale yellow solid residue with cold pentane (2×10 mL), ${}^{\text{ArF}}\text{PQpy}$ was obtained as an off-white solid (890 mg, 1.56 mmol, 89% yield). ${}^{31}\text{P}$ NMR (202 MHz, CD_2Cl_2): δ -58.19 (1P, quin, ${}^3J_{\text{P-F}} = 38$); ${}^{19}\text{F}$ NMR (470.4 MHz, CD_2Cl_2): δ -129.42 (2F, m); -150.69 (1F, t, ${}^3J_{\text{F-F}} = 20.4$); -161.37 (2F, m); ${}^1\text{H}$ NMR (500 MHz, CD_2Cl_2): δ 8.69 (1H, d, $J_{\text{H-H}} = 8.6$); 8.68 (1H, m); 8.37 (1H, d, $J_{\text{H-H}} = 8.6$); 8.09 (1H, d, $J_{\text{H-H}} = 8.0$); 7.98 (1H, dt, $J_{\text{H-H}} = 8.0$, $J_{\text{H-H}} = 1.1$); 7.75 (1H, td, $J_{\text{H-H}} = 7.7$, $J_{\text{H-H}} = 1.8$); 7.54 (1H, td, $J_{\text{H-H}} = 7.6$, $J_{\text{H-H}} = 1.7$); 7.42 (1H, dd, $J_{\text{H-H}} = 6.8$, $J_{\text{H-H}} = 4.1$); 7.34 (1H, dd, $J_{\text{H-H}} = 7.6$, $J_{\text{H-H}} = 4.6$).

${}^{\text{Mes}}\text{NQpy}$. 8-Acetyl-2-(pyrid-2'-yl)quinoline (0.496 g, 2 mmol) was mixed with 2,4,6-trimethylaniline (0.324 g, 2.4 mmol) and *p*-toluene sulfonic acid (0.017 g, 0.1 mmol) in toluene (40 mL). The resulting mixture was refluxed for 24 h to yield a dark yellow solution. The solution was evaporated to dryness, and the crude product was purified by chromatography using basic alumina, eluting with ethyl acetate (1–10%)/petroleum ether. The second fraction from the column gives the desired yellow colored product (0.51 g, 70% yield). ${}^1\text{H}$ NMR (500 MHz, CDCl_3): δ 2.26 (s, 6 H); 2.34 (s, 3 H); 2.41 (s, 3 H); 6.96 (s, 2 H); 7.35–7.39 (m, 1 H); 7.64 (dd, $J = 7.93$, 7.02 Hz, 1 H); 7.85 (td, $J = 7.78$, 1.83 Hz, 1 H); 7.93 (dd, $J = 8.09$, 1.37 Hz, 1 H); 8.00 (dd, $J = 7.02$, 1.53 Hz, 1 H); 8.34 (d, $J = 8.85$ Hz, 1 H); 8.58 (dt, $J = 8.01$, 1.03 Hz, 1 H); 8.67 (d, $J = 8.55$ Hz, 1 H); 8.74–8.77 (m, 1 H).

$\text{FeBr}_2({}^i\text{PrPQpy})$. A slurry of FeBr_2 (0.216 g, 1 mmol) in 5 mL of THF was added to a solution of ${}^i\text{PrPQpy}$ (0.322 g, 1 mmol) in 20 mL of THF. After stirring for 1 h, the reaction mixture was flooded with pentane to precipitate a green solid. X-ray quality crystals were obtained from vapor diffusion of pentane into a CH_2Cl_2 solution of the complex. ${}^1\text{H}$ NMR (500 MHz, CD_2Cl_2): δ 181.55 (2H, s); 144.23 (1H, s); 85.32 (1H, s); 79.04 (1H, s); 56.52 (1H, s); 27.12 (1H, s); 25.77 (1H, s); 15.69 (1H, s); 14.28 (1H, s); 10.00 (6H, s); 3.88 (6H, s); -20.1 (1H, s). Anal. Calcd for $\text{C}_{20}\text{H}_{23}\text{Br}_2\text{FeN}_2\text{P}$ (found): C, 44.65 (44.90); H, 4.31 (4.38); N, 5.21 (5.18). The yields of this and other metal complexes were 70–90%.

$\text{FeBr}_2({}^{\text{ArF}}\text{PQpy})$. This complex was prepared as described for $\text{FeBr}_2({}^i\text{PrPQpy})$. X-ray quality crystals were obtained by two steps: slow evaporation of a CH_2Cl_2 solution of the complex yields crystalline products, which were dissolved in THF, and the vapor diffusion of pentane into the THF solution of the complex generates X-ray quality crystals. Anal. Calcd for $\text{C}_{27.5}\text{H}_{12}\text{Br}_2\text{Cl}_3\text{F}_{10}\text{FeN}_2\text{P}$ ($\text{FeBr}_2({}^{\text{ArF}}\text{PQpy}) \cdot 1.5 \text{CH}_2\text{Cl}_2$) (found): C, 36.16 (35.77); H, 1.32 (1.18); N, 3.07 (3.33). When the reaction solution was allowed to stir for 2–3 h, a red solid precipitated. The red form of " $\text{FeBr}_2({}^{\text{ArF}}\text{PQpy})$ " is poorly soluble in THF and is assumed to be $[\text{Fe}({}^{\text{ArF}}\text{PQpy})_2] \cdot [\text{FeBr}_4]$.

$\text{CoCl}_2({}^i\text{PrPQpy})$. A slurry of CoCl_2 (0.130 g, 1 mmol) in 5 mL of THF was added to a solution of ${}^i\text{PrPQpy}$ (0.322 g, 1 mmol) in 20 mL of THF. After stirring for 1 h at room temperature, the reaction mixture was flooded with pentane to precipitate a gray-green solid. X-ray quality crystals were obtained by two methods: (i) vapor diffusion of pentane into CH_2Cl_2 solution of the complex and (ii) slow evaporation of a C_6D_6 solution of the complex. ${}^1\text{H}$ NMR (500 MHz, CD_2Cl_2): δ 127.36 (2H, s); 78.25 (1H, s); 74.75 (1H, s); 57.25 (1H, s); 39.62 (1H, s); 18.19 (1H, s); 17.39 (1H, s); 17.00 (1H, s); 10.30 (1H, s); -7.61 (1H, s); -12.80 (6H, s); -25.16 (6H, s). Anal. Calcd for $\text{C}_{20.5}\text{H}_{24}\text{Cl}_3\text{CoN}_2\text{P}$ [$\text{CoCl}_2({}^i\text{PrPQpy}) \cdot 0.5 \text{CH}_2\text{Cl}_2$] (found): C, 49.77 (49.26); H, 4.89 (4.67); N, 5.66 (5.53).

$\text{CoBr}_2({}^i\text{PrPQpy})$. A slurry of CoBr_2 (0.219 g, 1 mmol) in 5 mL of THF was added to a solution of ${}^i\text{PrPQpy}$ (0.322 g, 1 mmol) in 20 mL of THF. After stirring for 1 h, the reaction mixture was flooded with pentane to precipitate the blue-green solid. X-ray quality crystals were obtained from vapor diffusion of pentane into the CH_2Cl_2 solution of the complex. ${}^1\text{H}$ NMR (500 MHz, CD_2Cl_2): δ 66.54 (2H, s); 56.90 (1H, s); 44.00 (1H, s); 36.67 (1H, s); 26.55 (1H, s); 21.63 (1H, s); 20.89 (1H, s); 13.59 (1H, s); 10.26 (1H, s); 0.80 (1H, s); -3.74 (6H, s); -12.79 (6H, s). Anal. Calcd for $\text{C}_{20}\text{H}_{23}\text{Br}_2\text{CoN}_2\text{P}$ (found): C, 44.39 (44.28); H, 4.28 (4.24); N, 5.18 (4.61).

$\text{CoCl}_2({}^{\text{ArF}}\text{PQpy})$. A slurry of CoCl_2 (0.130 g, 1 mmol) in 5 mL of THF was added to a solution of ${}^{\text{ArF}}\text{PQpy}$ (0.570 g, 1 mmol) in 20 mL of THF. After stirring for 1 h at room temperature, the solution was flooded with pentane to precipitate a green solid. X-ray quality crystals were obtained from vapor diffusion of pentane into the CH_2Cl_2 solution of the complex, followed by vapor diffusion of Et_2O into the acetonitrile solution of the complex. ${}^1\text{H}$ NMR (500 MHz, CD_2Cl_2): 120.28 (1H, s); 72.28 (1H, s); 63.21 (1H, s); 55.77 (1H, s); 43.55 (1H, s); 32.41 (1H, s); 21.88 (1H, s); 18.26 (1H, s); 17.16 (1H, s). Anal. Calcd for $\text{C}_{27.5}\text{H}_{12}\text{Cl}_5\text{F}_{10}\text{CoN}_2\text{P}$ [$\text{CoCl}_2({}^{\text{ArF}}\text{PQpy}) \cdot 1.5 \text{CH}_2\text{Cl}_2$] (found): C, 39.91 (39.78); H, 1.46 (1.33); N, 3.39 (3.62).

$\text{FeBr}_2({}^{\text{Mes}}\text{NQpy})$. A slurry of FeBr_2 (0.216 g, 1 mmol) in 5 mL of THF was added to a solution of ${}^{\text{Mes}}\text{NQpy}$ (0.365 g, 1 mmol) in 20 mL of THF. After stirring for 1 h, the reaction mixture was flooded with pentane to precipitate a green solid. X-ray quality crystals were obtained from vapor diffusion of pentane into a CH_2Cl_2 solution of the complex. ${}^1\text{H}$ NMR (500 MHz, CD_2Cl_2): δ 59.54, 53.56, 52.87, 43.32, 30.98, 26.34, 15.60, 13.89, 6.66, 0.95, -1.95, -2.28.

$\text{CoCl}_2({}^{\text{Mes}}\text{NQpy})$. A slurry of CoCl_2 (0.130 g, 1 mmol) in 5 mL of THF was added to a solution of ${}^{\text{Mes}}\text{NQpy}$ (0.365 g, 1 mmol) in 20 mL of THF. After stirring for 1 h at room temperature, the reaction mixture was flooded with pentane to precipitate a yellow solid. X-ray quality crystals were obtained either by slow evaporation of CD_2Cl_2 solution or by vapor diffusion of pentane to the dichloromethane solution of the complex. ${}^1\text{H}$ NMR (500 MHz, CD_2Cl_2): δ 66.05, 64.81, 63.06, 59.48, 40.06, 37.00, 34.97, 22.30, 20.86, 17.86, 14.89, 14.44, 13.97, 13.69, 12.84, -5.35. Anal. Calcd for $\text{C}_{25.5}\text{H}_{24}\text{Cl}_3\text{CoN}_3$ [$\text{CoCl}_2({}^{\text{Mes}}\text{NQpy}) \cdot 0.5 \text{CH}_2\text{Cl}_2$] (found): C, 56.95 (57.26); H, 4.50 (4.03); N, 7.81 (7.59).

X-ray Crystallographic Determinations. Data for $\text{FeBr}_2({}^i\text{PrPQpy})$, $\text{FeBr}_2({}^{\text{ArF}}\text{PQpy})$, $\text{CoCl}_2({}^i\text{PrPQpy})$, $\text{CoBr}_2({}^i\text{PrPQpy})$, $\text{CoCl}_2({}^{\text{ArF}}\text{PQpy})$, $\text{FeBr}_2({}^{\text{Mes}}\text{NQpy})$, and $\text{CoCl}_2({}^{\text{Mes}}\text{NQpy})$ were collected on a Bruker D8 Venture instrument equipped with a four-circle kappa diffractometer and Photon 100 detector. An $I\mu\text{s}$ microfocus Mo ($\lambda = 0.71073 \text{ \AA}$) source supplied the multimirror monochromated incident beam. The samples were mounted on a 0.3 mm loop with the minimal amount of Paratone-N oil. Data were

collected as a series of φ and/or ω scans. Data were collected at 100 K and integrated and filtered for statistical outliers using SAINT (Bruker, 2014), and then, they were corrected for absorption by multiscan methods using SADABS v2014/7. The structures were phased using direct methods or intrinsic phasing methods and then refined with the SHELX software package SHELX-2014-7.^{52,53}

Catalysis with Liquid Alkenes. Substrates (alkene and silane) were mixed in a scintillation vial in the presence of the catalyst with or without solvent. The activator NaBHET₃ was added. After the reaction, the solution was opened to air to quench the reaction, and the NMR spectrum was recorded to establish the product distribution. In some cases, reactions were conducted in J-Young NMR tubes.

Catalysis with Gaseous Alkenes. Catalyst and silane were mixed in toluene in an 85 mL Fischer–Porter reactor in the presence of a measured amount of mesitylene as an NMR integration standard. Into the reaction solution was injected NaBHET₃ (2.2 equiv) as a toluene solution. The reactor was removed from the box, the solution was frozen, and the headspace evacuated and refilled with ethylene (2 atm). The solution was heated at 70 °C at 2 atm of ethylene. After 2 h, the solution was exposed to air to quench the reaction and filtered through a plug of silica gel. Volatiles were removed under a vacuum. A similar methodology was used for propylene. Experiments were performed in a 50 mL Schlenk tube, and the propylene gas was purged for 20 min prior to starting the catalytic reaction by injection of NaBHET₃.

■ ASSOCIATED CONTENT

● Supporting Information

The Supporting Information is available free of charge on the ACS Publications website at DOI: 10.1021/acs.organomet.8b00416.

Spectroscopic and crystallographic data (PDF)

Accession Codes

CCDC 1849756–1849762 and 1849762 contain the supplementary crystallographic data for this paper. These data can be obtained free of charge via www.ccdc.cam.ac.uk/data_request/cif, or by emailing data_request@ccdc.cam.ac.uk, or by contacting The Cambridge Crystallographic Data Centre, 12 Union Road, Cambridge CB2 1EZ, UK; fax: +44 1223 336033.

■ AUTHOR INFORMATION

Corresponding Author

*E-mail: rauchfuz@illinois.edu.

ORCID

Danielle L. Gray: 0000-0003-0059-2096

Thomas B. Rauchfuss: 0000-0003-2547-5128

Notes

The authors declare no competing financial interest.

■ ACKNOWLEDGMENTS

This research was funded by contract DEFG02-90ER14146 with the U.S. Department of Energy by its Division of Chemical Sciences, Geosciences, and Biosciences Division, Office of Basic Energy Sciences (D.B.), the Dow Chemical Company (R.G.-W., A.K.D.), and the National Science Foundation (T.B.R., D.B.). We thank Drs. Loren Durfee and Dimi Katsoulis for advice.

■ REFERENCES

- (1) Leeuwen, P. W. N. M. *Homogeneous Catalysis: Understanding the Art*; Kluwer: Dordrecht, The Netherlands, 2004.
- (2) Tondreau, A. M.; Atienza, C. C. H.; Weller, K. J.; Nye, S. A.; Lewis, K. M.; Delis, J. G. P.; Chirik, P. J. Iron Catalysts for Selective

Anti-Markovnikov Alkene Hydrosilylation Using Tertiary Silanes. *Science* **2012**, *335*, 567–570.

(3) Bart, S. C.; Lobkovsky, E.; Chirik, P. J. Preparation and Molecular and Electronic Structures of Iron(0) Dinitrogen and Silane Complexes and Their Application to Catalytic Hydrogenation and Hydrosilylation. *J. Am. Chem. Soc.* **2004**, *126*, 13794–13807.

(4) Peng, D.; Zhang, Y.; Du, X.; Zhang, L.; Leng, X.; Walter, M. D.; Huang, Z. Phosphinite-Iminopyridine Iron Catalysts for Chemo-selective Alkene Hydrosilylation. *J. Am. Chem. Soc.* **2013**, *135*, 19154–19166.

(5) Du, X.; Zhang, Y.; Peng, D.; Huang, Z. Base Metal-Catalyzed Regiodivergent Alkene Hydrosilylations. *Angew. Chem., Int. Ed.* **2016**, *55*, 6671–6675.

(6) Noda, D.; Tahara, A.; Sunada, Y.; Nagashima, H. Non-Precious-Metal Catalytic Systems Involving Iron or Cobalt Carboxylates and Alkyl Isocyanides for Hydrosilylation of Alkenes with Hydrosiloxanes. *J. Am. Chem. Soc.* **2016**, *138*, 2480–2483.

(7) Zuo, Z.; Yang, J.; Huang, Z. Cobalt-Catalyzed Alkyne Hydrosilylation and Sequential Vinylsilane Hydroboration with Markovnikov Selectivity. *Angew. Chem., Int. Ed.* **2016**, *55*, 10839–10843.

(8) Hayasaka, K.; Kamata, K.; Nakazawa, H. Highly Efficient Olefin Hydrosilylation Catalyzed by iron Complexes with Iminobipyridine Ligand. *Bull. Chem. Soc. Jpn.* **2016**, *89*, 394–404.

(9) Ibrahim, A. D.; Entsminger, S. W.; Zhu, L.; Fout, A. R. A highly chemoselective Cobalt Catalyst for the Hydrosilylation of Alkenes Using Tertiary Silanes and Hydrosiloxanes. *ACS Catal.* **2016**, *6*, 3589–3593.

(10) Pappas, I.; Treacy, S.; Chirik, P. J. Alkene Hydrosilylation Using Tertiary Silanes with α -Diimine Nickel Catalysts. Redox-Active Ligands Promote a Distinct Mechanistic Pathway from Platinum Catalysts. *ACS Catal.* **2016**, *6*, 4105–4109.

(11) Chen, C.; Hecht, M. B.; Kavara, A.; Brennessel, W. W.; Mercado, B. Q.; Weix, D. J.; Holland, P. L. Rapid, Regioconvergent, Solvent-Free Alkene Hydrosilylation with a Cobalt Catalyst. *J. Am. Chem. Soc.* **2015**, *137*, 13244–13247.

(12) Nakajima, Y.; Shimada, S. Hydrosilylation reaction of olefins: recent advances and perspectives. *RSC Adv.* **2015**, *5*, 20603–20616.

(13) Nakajima, Y.; Sato, K.; Shimada, S. Development of Nickel Hydrosilylation Catalysts. *Chem. Rec.* **2016**, *16*, 2379–2387.

(14) Obligacion, J. V.; Chirik, P. J. Earth-abundant Transition Metal Catalysts for Alkene Hydrosilylation and Hydroboration. *Nature Rev. Chem.* **2018**, *2*, 15–34.

(15) Schuster, C. H.; Diao, T.; Pappas, I.; Chirik, P. J. Bench-Stable, Substrate-Activated Cobalt Carboxylate Pre-Catalysts for Alkene Hydrosilylation with Tertiary Silanes. *ACS Catal.* **2016**, *6*, 2632–2636.

(16) Gilbert-Wilson, R.; Chu, W.-Y.; Rauchfuss, T. B. Phosphine-Iminopyridines as Platforms for Catalytic Hydrofunctionalization of Alkenes. *Inorg. Chem.* **2015**, *54*, 5596–5603.

(17) Chu, W.-Y.; Gilbert-Wilson, R.; Rauchfuss, T. B.; van Gestel, M.; Neese, F. Cobalt Phosphino- α -Iminopyridine-Catalyzed Hydrofunctionalization of Alkenes: Catalyst Development and Mechanistic Analysis. *Organometallics* **2016**, *35*, 2900–2914.

(18) Gunanathan, C.; Milstein, D. Metal-Ligand Cooperation by Aromatization-De aromatization: A New Paradigm in Bond Activation and “Green” Catalysis. *Acc. Chem. Res.* **2011**, *44*, 588–602.

(19) Zell, T.; Milstein, D. Hydrogenation and Dehydrogenation Iron Pincer Catalysts Capable of Metal-Ligand Cooperation by Aromatization/De aromatization. *Acc. Chem. Res.* **2015**, *48*, 1979–1994.

(20) Zhang, L.; Zuo, Z.; Leng, X.; Huang, Z. A Cobalt-Catalyzed Alkene Hydroboration with Pinacolborane. *Angew. Chem., Int. Ed.* **2014**, *53*, 2696–2700.

(21) Wu, J. Y.; Moreau, B.; Ritter, T. Iron-Catalyzed 1,4-Hydroboration of 1,3-Dienes. *J. Am. Chem. Soc.* **2009**, *131*, 12915–12917.

(22) Parker, S. E.; Borgel, J.; Ritter, T. 1,2-Selective Hydrosilylation of Conjugated Dienes. *J. Am. Chem. Soc.* **2014**, *136*, 4857–4860.

- (23) Kamata, K.; Suzuki, A.; Nakai, Y.; Nakazawa, H. Catalytic Hydrosilylation of Alkenes by Iron Complexes Containing Terpyridine Derivatives as Ancillary Ligands. *Organometallics* **2012**, *31*, 3825–3828.
- (24) Tong, L.; Zong, R.; Thummel, R. P. Visible Light-Driven Hydrogen Evolution from Water Catalyzed by A Molecular Cobalt Complex. *J. Am. Chem. Soc.* **2014**, *136*, 4881–4884.
- (25) Wickramasinghe, L. D.; Zhou, R.; Zong, R.; Vo, P.; Gagnon, K. J.; Thummel, R. P. Iron Complexes of Square Planar Tetradentate Polypyridyl-Type Ligands as Catalysts for Water Oxidation. *J. Am. Chem. Soc.* **2015**, *137*, 13260–13263.
- (26) LeBlanc, F. A.; Piers, W. E.; Parvez, M. Selective Hydrosilylation of CO₂ to a Bis(silylacetel) Using an Anilido Bipyridyl-Ligated Organoscandium Catalyst. *Angew. Chem., Int. Ed.* **2014**, *53*, 789–792.
- (27) Mao, L.; Moriuchi, T.; Sakurai, H.; Fujii, H.; Hirao, T. New Tridentate Cyclometalated Platinum(II) and Palladium(II) Complexes of *N*,2-Diphenyl-8-quinolinamine: Syntheses, Crystal Structures, and Photophysical Properties. *Tetrahedron Lett.* **2005**, *46*, 8419–8422.
- (28) Sacconi, L.; Bertini, I. Low- and High-Spin Five-Coordinate Cobalt(II) and Nickel(II) Complexes with Tris(2-diphenylphosphinoethyl)amine. *J. Am. Chem. Soc.* **1968**, *90*, 5443–5446.
- (29) Goodwin, H. A. In *Spin Crossover in Transition Metal Compounds II*; Gütllich, P., Goodwin, H. A., Eds.; Springer: 2004.
- (30) Addison, A. W.; Rao, T. N.; Reedijk, J.; van Rijn, J.; Verschoor, G. C. Synthesis, Structure, and Spectroscopic Properties of Copper(II) Compounds Containing Nitrogen-Sulphur Donor Ligands; the Crystal and Molecular Structure of Aqua[1,7-bis(N-methylbenzimidazol-2'-yl)-2,6-dithiaheptane]copper(II) Perchlorate. *J. Chem. Soc., Dalton Trans.* **1984**, 1349–1356.
- (31) Atienza, C. C. H.; Diao, T.; Weller, K. J.; Nye, S. A.; Lewis, K. M.; Delis, J. G. P.; Boyer, J. L.; Roy, A. K.; Chirik, P. J. Bis(imino)pyridine Cobalt-Catalyzed Dehydrogenative Silylation of Alkenes: Scope, Mechanism, and Origins of Selective Allylsilane Formation. *J. Am. Chem. Soc.* **2014**, *136*, 12108–12118.
- (32) Marciniak, B.; Gulinski, J. Catalysis of Hydrosilylation. VII. Catalysis of Hydrosilylation of Carbon-Carbon Double Bonds by Ruthenium Phosphine Complexes. *J. Organomet. Chem.* **1983**, *253*, 349–362.
- (33) Takeuchi, R.; Ishii, N.; Sugiura, M.; Sato, N. The Highly Regioselective Carbonylation of Vinylsilanes. *J. Org. Chem.* **1992**, *57*, 4189–4194.
- (34) Pietraszuk, C.; Marciniak, B.; Fischer, H. Cross-Metathesis of Vinylsilanes with Styrene Catalyzed by Ruthenium-Carbene Complexes. *Organometallics* **2000**, *19*, 913–917.
- (35) Pawluc, P.; Prukala, W.; Marciniak, B. Silylative Coupling of Olefins with Vinylsilanes in the Synthesis of π -Conjugated Double Bond Systems. *Eur. J. Org. Chem.* **2010**, *2010*, 219–229.
- (36) Lu, B.; Falck, J. R. Iridium-Catalyzed (*Z*)-Trialkylsilylation of Terminal Olefins. *J. Org. Chem.* **2010**, *75*, 1701–1705.
- (37) Rivera-Hernández, A.; Fallon, B. J.; Ventre, S.; Simon, C.; Tremblay, M.-H.; Gontard, G.; Derat, E.; Amatore, M.; Aubert, C.; Petit, M. Regio- and Stereoselective Hydrosilylation of Unsymmetrical Alkynes Catalyzed by a Well-Defined, Low-Valent Cobalt Catalyst. *Org. Lett.* **2016**, *18*, 4242–4245.
- (38) Liu, L.; Li, X.; Dong, H.; Wu, C. Hydrosilylation Reaction of Ethylene with Triethoxysilane Catalyzed by Ruthenium Halides and promoted by Cuprous Halides. *J. Organomet. Chem.* **2013**, *745–746*, 454–459.
- (39) Chernyshev, E. A.; Belyakova, Z. V.; Knyazev, S. P.; Turkel'taub, G. N.; Parshina, E. V.; Serova, I. V.; Storozhenko, P. A. Hydrosilylation of ethylene. *Russ. J. Gen. Chem.* **2006**, *76*, 225–228.
- (40) Quirk, J. M.; Kanner, B. Process for the Preparation of Olefinic Silanes and Siloxanes, US4668812A, Union Carbide Corp., 1987.
- (41) Barbero, A.; Pulido, F. J. Allylsilanes and Vinylsilanes from Silylcupration of Carbon-Carbon Multiple Bonds: Scope and Synthetic Applications. *Acc. Chem. Res.* **2004**, *37*, 817–825.
- (42) Sarkar, T. K. Methods for the Synthesis of Allylsilanes. *Synthesis* **1990**, *1990*, 1101–1111.
- (43) Luh, T.-Y.; Liu, S.-T. In *Chemistry of Organic Silicon Compounds*; Rappoport, Z., Apeloig, Y., Eds.; Wiley: 1998.
- (44) Diao, T.; Chirik, P. J.; Roy, A. K.; Lewis, K.; Nye, S.; Weller, K. J.; Delis, J. G. P.; Yu, R. Dehydrogenative Silylation, Hydrosilylation and Crosslinking Using Cobalt Catalysts, Momentive Performance Materials and Princeton University, 2015.
- (45) Sakaki, S.; Mizoe, N.; Sugimoto, M. Theoretical Study of Platinum(0)-Catalyzed Hydrosilylation of Ethylene. Chalk–Harrod Mechanism or Modified Chalk–Harrod Mechanism. *Organometallics* **1998**, *17*, 2510–2523.
- (46) Fegley, G. J.; Larson, G. L. *Encycl. Reag. Org. Synth.*; John Wiley & Sons: New York, 2008.
- (47) Wolff, S. K. Chemical Aspects of Rubber Reinforcement by Fillers. *Rubber Chem. Technol.* **1996**, *69*, 325–346.
- (48) Christ, M. L.; Sabo-Etienne, S.; Chaudret, B. Highly Selective Dehydrogenative Silylation of Ethylene Using the Bis(dihydrogen) Complex RuH₂(H₂)₂(PCy₃)₂ as Catalyst Precursor. *Organometallics* **1995**, *14*, 1082–1084.
- (49) LaPointe, A. M.; Rix, F. C.; Brookhart, M. Mechanistic Studies of Palladium(II)-Catalyzed Hydrosilylation and Dehydrogenative Silylation Reactions. *J. Am. Chem. Soc.* **1997**, *119*, 906–917.
- (50) Jiang, Y.; Blacque, O.; Fox, T.; Freche, C. M.; Berke, H. Highly Selective Dehydrogenative Silylation of Alkenes Catalyzed by Ruthenium Complexes. *Chem. - Eur. J.* **2009**, *15*, 2121–2128.
- (51) Marciniak, B. Dehydrogenative Coupling of olefins with silicon compounds Catalyzed by Transition-Metal Complexes. *New J. Chem.* **1997**, *21*, 815–824.
- (52) Krause, L.; Herbst-Irmer, R.; Sheldrick, G. M.; Stalke, D. Comparison of silver and Molybdenum Microfocus X-ray Sources for single-crystal structure determination. *J. Appl. Crystallogr.* **2015**, *48*, 3–10.
- (53) Sheldrick, G. M. SHELXT - Integrated Space-Group and Crystal-Structure Determination. *Acta Crystallogr., Sect. A: Found. Adv.* **2015**, *71*, 3–8.